# The Influence of a Critical Latitude on Topographically Forced Stationary Waves in a Barotropic Model

SUMANT NIGAM

*Geophysical Fluid Dynamics Program, Princeton University, Princeton, NJ 08540*

ISAAC M. HELD

*Geophysical Fluid Dynamics Laboratory/NOAA, Princeton University, Princeton, NJ 08540*

(Manuscript received 19 April 1983, in final form 13 July 1983)

ABSTRACT

A nondivergent barotropic model on a sphere is used to study the effects of a critical latitude on stationary atmospheric waves forced by topography. Linear and "quasi-linear" calculations are performed with an idealized wavenumber 3 mountain and with realistic topography. Quasi-linear dynamics, where mean flow changes are due to momentum flux convergence, "form drag" and relaxation to a prescribed climatological mean flow, produces an S-shaped kink in the zonal mean absolute vorticity gradient near the critical latitude, resulting in enhanced reflection. The component of the quasi-linear solution resulting from enhanced reflection at the critical latitude is computed by taking the difference between the linear and the quasi-linear solutions. In a calculation with realistic topography and zonal flow, this reflected component is found to be dominated by a wave train emanating from the western tropical Pacific and propagating northward and then eastward across the Pacific Ocean and the North American continent. This wave train results from the reflection of the Himalayan wave train at the zero-wind latitude in the tropical winter troposphere.

The vorticity gradients in the monthly mean statistics of Oort (1983) show structure near the critical latitude similar to that produced in our quasi-linear model, suggesting that some reflection of incident Rossby waves is likely in the atmosphere, at least in the western Pacific, and that the wind structure responsible for this reflection may be created in part by the stationary Rossby waves themselves.

## 1. Introduction

Stationary Rossby waves forced in midlatitudes and trapped within the troposphere are typically refracted into low latitudes, where they often encounter a transition from westerlies to easterlies. At this critical latitude (CL), the theory for linear inviscid and steady waves breaks down. Whether this breakdown results primarily in absorption or reflection of the incident waves is of vital importance for the extratropical wave problem.

The wave is at least partially absorbed at the critical latitude if diffusion or damping of eddy vorticity is used to remove the critical latitude singularity for meridionally propagating Rossby waves (Kuo, 1949; Dickinson, 1968). A similar result emerges when the initial value approach is used to solve the linear inviscid Rossby wave critical latitude problem for a linear shear flow (Dickinson, 1970; Yamagata, 1976). In contrast, Benney and Bergeron (1969) find a solution with nonlinearity rather than dissipation dominant near the critical latitude, in which the wave is perfectly reflected. The quasi-linear inviscid calculations of Geisler and Dickinson (1974) and Beland (1976) also show the Rossby wave CL to be perfectly reflecting in the steady state, indicating that a simple wave–mean flow interaction model can capture the essence of the reflection mechanism despite its arbitrary truncation of the full equations and the resulting distortion of the solution in the immediate vicinity of the critical latitude. Analytic work of Haberman (1972) and Tung (1979) shows the ratio of nonlinearity to viscosity to be the key parameter which decides whether the CL reflects or absorbs the incident Rossby waves. These conclusions are supported by the numerical calculations of Beland (1978) in which the fully nonlinear barotropic vorticity equation is integrated forward in time for a range of viscosity coefficients. Beland also shows that for realistic parameter values it takes the flow in the vicinity of the CL about a week to attain a strongly reflecting structure. Tung (1979) has argued that the Rossby wave CL in the real atmosphere is dominated by nonlinearities and must therefore reflect incident stationary wave energy. These results have led to a renewed interest in exploring the possibility of Rossby wave resonance in the real atmosphere.

Grose and Hoskins (1979) describe the steady linear response to flow over realistic topography using the shallow water equations on a sphere. These solutions and their close relationship to analogous solutions in

baroclinic models have been discussed further in Hoskins and Karoly (1981) and Held (1983). In this paper we examine how this linear response is modified when stationary waves are allowed to interact with the zonal mean flow and topography. The zonal mean flow is not completely free to respond to these interactions as its departure from its climatological value is constrained by the presence of a relaxation term. The only dissipative effect in the model is a linear drag which acts everywhere. The strongest interaction is expected to occur near the critical latitude and to result in enhanced reflection, as described by Geisler and Dickinson.

The model formulation is described in Section 2 while some theoretical preliminaries are discussed in Section 3. The effect of the CL on the structure and character of stationary waves forced by an idealized wavenumber 3 mountain is described in Section 4 and of those forced by realistic topography in Section 5. Aspects of the observed tropical flow field which suggest that it is capable of reflecting incident Rossby waves, at least in the western Pacific, are described in Section 6. Discussion and conclusions follow in Section 7.

## 2. Model formulation

Consider quasi-geostrophic flow in a homogeneous, incompressible and hydrostatic atmosphere which is bounded at the top by a rigid lid. Such a model conserves potential vorticity following horizontal fluid motion. The horizontal flow in our model is damped everywhere by a linear drag while the axially symmetric zonal flow is forced to relax to a specified climatological profile $\bar{U}_e$. The equation describing the motion is

$$\frac{d}{dt}\left(\frac{\zeta+f}{H}\right)=\frac{D}{H}(\bar{\zeta}_e-\zeta), \tag{1}$$

where

| | |
|---|---|
| $\frac{d}{dt}$ | horizontal material derivative |
| $\zeta$ | relative vorticity |
| $\bar{\zeta}_e$ | zonal mean climatological vorticity |
| $f$ | Coriolis parameter [$=2\Omega\sin\theta$] |
| $D$ | drag coefficient |
| $H_0$ | height of the rigid lid |
| $h(\lambda, \theta)$ | surface topography [$h/H_0 < 1$] |
| $H(\lambda, \theta)$ | height of the fluid column [$=H_0 - h(\lambda, \theta)$] |
| $\lambda, \theta$ | longitude and latitude respectively. |

The equation for the zonally symmetric flow $\bar{U}$ is obtained by integrating (1) with respect to $\theta$ and then averaging over $\lambda$ to give

$$\frac{\partial\bar{U}}{\partial t}=\overline{v'\zeta'}+\frac{f}{H_0}\overline{v'h'}+D(\bar{U}_e-\bar{U}), \tag{2a}$$

where the overbar denotes the zonal mean and the prime the deviation from it. Here

$$\overline{v'\zeta'}=-\frac{1}{a\cos\theta}\frac{\partial\{\overline{u'v'}\cos\theta\}}{\partial\theta}$$

is the eddy momentum flux convergence, $(f/H_0)\overline{v'h'}$ is the "form drag" or the mountain torque and $D(\bar{U}_e - \bar{U})$ is the relaxation term.

The equation for the zonally asymmetric part of the flow is obtained by linearizing (1) after subtracting its zonal mean

$$\frac{\partial\zeta'}{\partial t}+\frac{\bar{U}}{a\cos\theta}\frac{\partial\zeta'}{\partial\lambda}+v'\left(\beta+\frac{1}{a}\frac{\partial\bar{\zeta}}{\partial\theta}\right)=-\frac{f}{H_0}\left(\frac{\bar{U}}{a\cos\theta}\frac{\partial h'}{\partial\lambda}\right)-D\zeta', \tag{2b}$$

where

$\zeta'(\lambda, \theta)=\frac{1}{a^2}\left[\frac{1}{\cos^2\theta}\frac{\partial^2\psi'}{\partial\lambda^2}+\frac{1}{\cos\theta}\frac{\partial}{\partial\theta}\left(\cos\theta\frac{\partial\psi'}{\partial\theta}\right)\right]$, the eddy vorticity,

$u'=-\frac{1}{a}\frac{\partial\psi'}{\partial\theta}$, the eddy zonal velocity,

$v'=\frac{1}{a\cos\theta}\frac{\partial\psi'}{\partial\lambda}$, the eddy meridional velocity,

and $\psi'(\lambda, \theta)$ the eddy streamfunction, $a$ the radius of the earth, and $\beta = 2\Omega a^{-1}\cos\theta$, the planetary vorticity gradient.

Eqs. (2a) and (2b) form the quasi-linear system. In the linear calculation, $\bar{U}$ is prescribed and the steady state $\zeta'$ determined by solving (2b) as a boundary value problem. In the quasi-linear calculation $\bar{U}_e$ is specified in (2a) and the solutions $\zeta'$ and $\bar{U}$ are determined by integrating Eqs. (2) forward in time.

A semi-spectral model is constructed to numerically integrate the quasi-linear system. The model has a high meridional resolution having 401 grid points equally spaced between the North and the South Poles. The eddy vorticity is represented as

$$\zeta'(\lambda, \theta, t)=\sum_{m=1}^{M}2\,\mathrm{Re}[\tilde{\zeta}_m(\theta, t)\exp(im\lambda)], \tag{3}$$

where $\tilde{\zeta}_m(\theta, t)$ is the complex eddy vorticity amplitude of the $m$th wavenumber. The eddy streamfunction and topography are similarly represented. The Euler scheme is used to start the integration of (2) which is then carried forward using the leapfrog time scheme. The quasi-linear system is initialized by setting $\bar{U}=\bar{U}_e$ and $\tilde{\zeta}_m = 0.0$. At each time step, $\tilde{\zeta}_m$ is inverted to obtain $\tilde{\psi}_m$ by using the technique of Lindzen and Kuo (1969).

The drag coefficient $D$ is chosen to represent an $e$-folding damping time of 13.5 days and $H_0$ is set equal to 8000 m. Even though the model is global, the topography in all cases is confined to the Northern Hemisphere alone. The Appendix contains a detailed description of the difference equations resulting from time and meridional finite differencing of Eqs. (2) and

of the quantities that these difference equations conserve when inviscid and unforced.

## 3. Theoretical preliminaries

In this section, we summarize some relevant properties of Rossby waves on a latitude-dependent mean flow. On a $\beta$-plane, the equation determining the meridional structure of a linearly damped barotropic Rossby wave outside the region of forcing is

$$\frac{\partial^2\tilde{\psi}}{\partial y^2} + l^2(y, k)\tilde{\psi} = 0, \tag{4}$$

where

$\psi'(x, y, t) = 2\,\text{Real}\{\tilde{\psi}(y)e^{ik(x-ct)}\}$ is the eddy streamfunction;

$l^2(y, k) = \dfrac{\hat{\beta}}{\bar{U} - c - iDk^{-1}} - k^2$, the square of the meridional wavenumber,

$\hat{\beta}(y) = \beta - \dfrac{\partial^2\bar{U}}{\partial y^2}$, the zonal mean absolute vorticity gradient.

The phase velocity $c$ is real. Away from the critical latitude, where $\bar{U} = c$, the eddy momentum flux $u'v'$ is independent of latitude in the limit $D \to 0$. Latitudes at which $l = 0$ are referred to as turning latitudes. The phase $\Phi$ of $\tilde{\psi}$ is defined as

$$\Phi(y) = \tan^{-1}\left(\frac{\tilde{\psi}_i}{\tilde{\psi}_r}\right),$$

where the subscripts $i$ and $r$ denote the imaginary and real part respectively. The eddy momentum flux can now be expressed as

$$\overline{u'v'} = -2k|\tilde{\psi}|^2\frac{\partial\Phi}{\partial y}.$$

If the WKB approximation $\tilde{\psi} \approx l^{-1/2}\exp[\pm i\int l(\xi)d\xi]$ is valid; that is, if

$$l^{1/2}\frac{d^2}{dy^2}(l^{-1/2}) \ll l^2, \tag{5}$$

then one can speak of northward and southward propagating components of the wave. One finds that $u'v' > 0$ ($<0$) for southward (northward) propagation and that $u'v' = 0$ if the two components have equal amplitudes. There is a jump in $u'v'$ at the critical latitude $y_c$ (e.g., Lindzen and Tung, 1978), where

$$\overline{u'v'}|_{y_c+} - \overline{u'v'}|_{y_c-} = 2\pi k\left(\frac{\hat{\beta}|\tilde{\psi}|^2}{\partial\bar{U}/\partial y}\right)_{y_c}, \tag{6}$$

the transition occurring over a distance of the order of $D(k\partial\bar{U}/\partial y)^{-1}$. The value of $D$ chosen for the calculations described here, $(13.5\text{ days})^{-1}$, is sufficiently small that waves can propagate into the tropics and back to midlatitudes retaining significant amplitudes, while being sufficiently large that the momentum flux transition at $y_c$ is smoothly resolved by our numerical model.

In the simple case in which the wave is evanescent, $\text{Re}(l^2) < 0$ for all $y < y_c$, $u'v'|_{y_c-} = 0$ as $D \to 0$. If $\hat{\beta}$ happens to equal zero at $y = y_c$, then we also have $u'v'|_{y_c+} = 0$, implying perfect reflection of the incident wave. Geisler and Dickinson (1974) obtain near perfect reflection in their quasi-linear model because the wave-induced accelerations force $\hat{\beta}$ to zero at $y_c$. If $\hat{\beta}$ is greater than zero at $y_c$ is the wave partially reflected or totally absorbed at CL? One *smooth* and continuous flow profile which has been analytically investigated and for which one can answer the above question is the linear shear flow profile

$$\bar{U} = s(y - y_c); \quad s = \text{constant slope}.$$

Dickinson's (1968) analytic solutions for the equation

$$\frac{\partial^2\tilde{\psi}}{\partial y^2} = \frac{-\beta}{s(y - y_c)}\tilde{\psi}, \tag{7}$$

which determines the meridional structure of barotropic Rossby waves in a linear shear flow in the long wave limit, show the wave absorption to be essentially complete at CL. However, in the case of more general smooth and continuous flow profiles, the wave may be partially reflected at CL instead of being totally absorbed there. In particular, it appears that if there is no overlap between the region where the WKB approximation is valid and the region near the critical latitude where solutions are well represented by Eq. (7), then partial reflection is possible even in the linear problem. We return to this point in Section 4, as it is central to our interpretation of the solutions to be described.

When (2b) is rewritten in Mercator coordinates it is transformed into an equation isomorphic to the barotropic vorticity equation on a Cartesian $\beta$-plane (Kuo, 1949; Hoskins and Karoly, 1981); the new quantity analogous to $\hat{\beta}$ is

$$\beta_m = \frac{2\Omega\cos^2\theta}{a} - \frac{\cos\theta}{a^2}\frac{\partial}{\partial\theta}\left[\frac{1}{\cos\theta}\frac{\partial}{\partial\theta}(\bar{U}\cos\theta)\right]. \tag{8}$$

## 4. One wave experiment

In the calculations described in this section, the eddy fields and topography consist of a single zonal wave ($m = 3$). The mountain is located in midlatitudes in the Northern Hemisphere:

$$h(\lambda, \theta) = \hat{h}(\theta)\cos(m\lambda),$$

where

$$\hat{h}(\theta) = \begin{cases} h_0\sin\left[\dfrac{(\theta - 34.65°)\pi}{20.25°}\right], & 34.65° < \theta < 54.9° \\ 0, & \text{otherwise.} \end{cases}$$

For the first set of calculations, we set $\bar{U}_e(\theta) = U1(\theta)$, where $U1(\theta)$ is an idealized profile of the 300 mb zonal mean zonal wind during the Northern Hemisphere winter and is defined as

$$U1(\theta) = E \sin\left[\frac{3\pi}{2}(1. + \sin\theta)\right] + F(1. - \sin^2\theta), \quad (9)$$

with $E = 18$ m s$^{-1}$ and $F = 14$ m s$^{-1}$; the analytic expression is taken from Webster (1981). The $U1$ profile has a critical latitude at $\theta \approx 8.6°$N and a turning latitude for wavenumber 3 at $\theta \approx 58°$N. In the corresponding linear calculation, $\bar{U}$ is set equal to $U1(\theta)$. To isolate the influence of the CL on stationary waves, these calculations are repeated with another profile $U2(\theta)$ which is similar to $U1(\theta)$ but which does not have a critical latitude. This is obtained from (9) by setting $E = 15$ m s$^{-1}$ and $F = 18$ m s$^{-1}$.

### *a. Calculation with U1*

Figs. 1–7 describe results for $h_0 = 300$ m. The quasi-linear solution approaches a steady state as $t \to \infty$, and we find the same steady state for a variety of initial conditions. For this value of $h_0$, the stationary wave streamfunction amplitude is roughly a factor of 2–3 smaller than the observed deviations from zonal symmetry in the extratropical upper troposphere during winter. If one tries to increase the wave amplitude by increasing $h_0$ to 900 m, one finds that unrealistic mean flow is generated in low latitudes, a problem which we return to when discussing realistic topographic forcing in Section 5. If one tries to enhance the wave amplitude by decreasing the damping coefficient to (30 days)$^{-1}$, one finds that the wave amplitude responds only slightly (~15%).

Fig. 1 shows $\bar{U}$ and the associated $\beta_m$ in the linear and the quasi-linear steady states. The two profiles are indistinguishable in the Southern Hemisphere since very little wave activity penetrates through the tropical easterlies. In the quasi-linear case, the flow is decelerated mainly to the north of the critical latitude of the $U1$ profile, resulting in the northward displacement of the critical latitude by ~4°. The quasi-linear $\beta_m$ varies rapidly in a narrow band (an S-shaped structure) and is driven to quite small values near the critical latitude. The discussion in Section 3 would then lead one to expect enhanced reflection in the quasi-linear case. In contrast with Geisler's and Dickinson's study, $\beta_m$ does not vanish at the new critical latitude—presumably due to the restraining influence of the relaxation term $D(\bar{U}_e - \bar{U})$.

Fig. 2 shows the meridional structure of the eddy momentum flux. It is poleward (positive) south of the mountain and equatorward (negative) north of it, the direction of eddy momentum flux ($\underline{u'v'}$) being opposite to the direction of energy propagation for stationary waves in a westerly flow. North of the mountain, the eddy momentum flux has an exponentially decaying structure due to the presence of a turning latitude near 58°N. At and in the vicinity of the CL, $u'v'$ in the

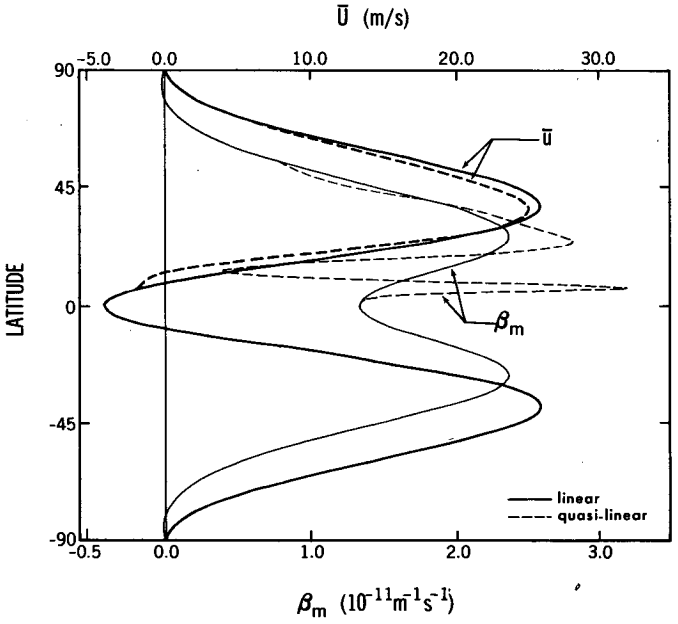


FIG. 1. Meridional structure of $\bar{U}$ and the associated $\beta_m$ in the linear and quasi-linear steady state. The thick solid line represents $\bar{U}$ while the thin solid line represents $\beta_m$ in the linear case. The corresponding dashed lines distinguish the quasi-linear solution from the linear in regions where the two differ.

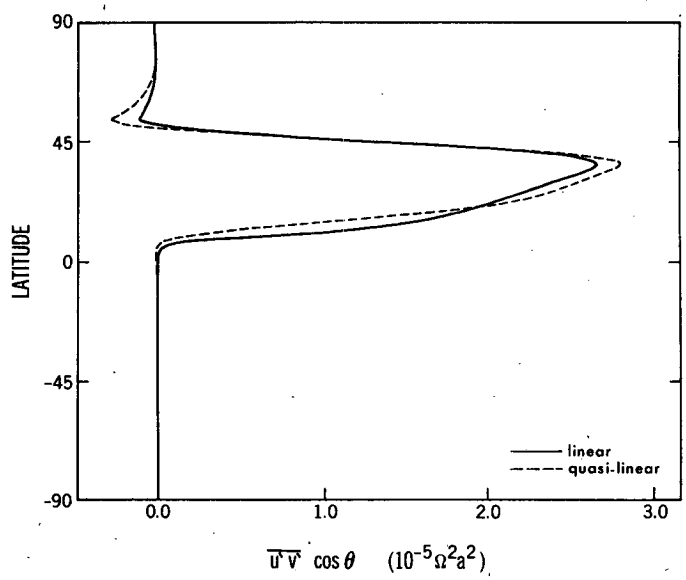


FIG. 2. Meridional structure of the eddy momentum flux. The dashed line distinguishes the quasi-linear case from the linear in regions where the two differ.

quasi-linear case is noticeably smaller than in the linear case (e.g., reducing from the linear value of 1.27 units to 0.6 units at 10°N), indicating that the quasi-linear steady CL is more reflecting.

Fig. 3a shows the eddy streamfunction amplitude and Fig. 3b the phase in the linear ($\tilde{\psi}_l$) and quasi-linear ($\tilde{\psi}_q$) calculations, as well as for their difference, ($\tilde{\psi}_q - \tilde{\psi}_l$). In the quasi-linear case, the amplitude is enhanced in low and middle latitudes and reduced in the subtropics. A similar subtropical minimum in amplitude and a phase change across the minimum are present in the observed wintertime stationary wave field (Lau, 1979). This structure in $\tilde{\psi}_q$ is suggestive of interference between equatorward and poleward propagating waves. Indeed, we see that the phase of $\tilde{\psi}_l$ decreases with increasing $\theta$, while that of $\tilde{\psi}_q - \tilde{\psi}_l$ increases, implying that $\tilde{\psi}_l$ and $\tilde{\psi}_q - \tilde{\psi}_l$ are dominated by equatorward and poleward propagating waves respectively. Fig. 4 is a plot of the correlation coefficient ($R$) defined as

$$R = \frac{\overline{u'v'}}{(\overline{u'^2}\,\overline{v'^2})^{1/2}}, \tag{10}$$

and computed for $\tilde{\psi}_l$ and $\tilde{\psi}_q$. Since $\tilde{\psi}_l$ yields a correlation of very near +1.0 between the source and the critical latitude, it consists in this region of an essentially pure equatorward propagating wave. In the neighborhood of the CL, the correlation coefficient in the quasi-linear case is reduced to ~0.4. This reduction in coherence between $u'$ and $v'$ is due to the presence of a poleward propagating wave ($\tilde{\psi}_q - \tilde{\psi}_l$), resulting from reflection of the incident wave $\tilde{\psi}_l$ at the CL.

Fig. 5 shows the balance between form drag, eddy momentum flux convergence, and mean flow relaxation in the quasi-linear steady state. Form drag is nonzero only in the region of the mountain, where its negative value implies that the trough is downwind of the mountain. The waves generated by the mountain redistribute this drag by removing angular momentum from low and (to a much lesser extent) from high latitudes. The sum of the form drag and eddy momentum flux convergence balances $D(\bar{U}_e - \bar{U})$. The midlatitude mountain is seen to retard the zonal flow throughout the Northern Hemisphere, as one might intuitively expect when an obstacle is placed in the path of a westerly current. Somewhat less intuitive is the result that the largest retardation, $(\bar{U}_e - \bar{U}) \approx 4.5$ m s$^{-1}$, occurs in low latitudes northward of the critical latitude.

Because of the interference between incident and reflected waves in the quasi-linear solution, one expects it to be more sensitive than the linear solution to variations in the strength and/or structure of the basic zonal flow. To illustrate this point, we vary $\bar{U}_e$ as follows:

$$\bar{U}_e(\theta) = [1. + \epsilon \sin^2(2\theta)]U1(\theta), \tag{11}$$

where $\epsilon$ ranges from −0.4 to +0.4. The nine profiles so generated are shown in Fig. 6. Fig. 7 shows domain averages of $|\tilde{\psi}_l|^2$, $|\tilde{\psi}_q|^2$ and $|\tilde{\psi}_q - \tilde{\psi}_l|^2$ as functions of $\epsilon$. The quasi-linear solution shows greater sensitivity than the linear solution, with a peak in sensitivity at $\epsilon = -0.1$ (a plot of total form drag as a function of $\epsilon$ is qualitatively similar). However, note that $|\tilde{\psi}_q - \tilde{\psi}_l|^2$ averaged over the domain shows no structure as a function of $\epsilon$. This suggests that the peak in amplitude at $\epsilon = -0.1$ does not represent a resonance but is simply the result of constructive interference between

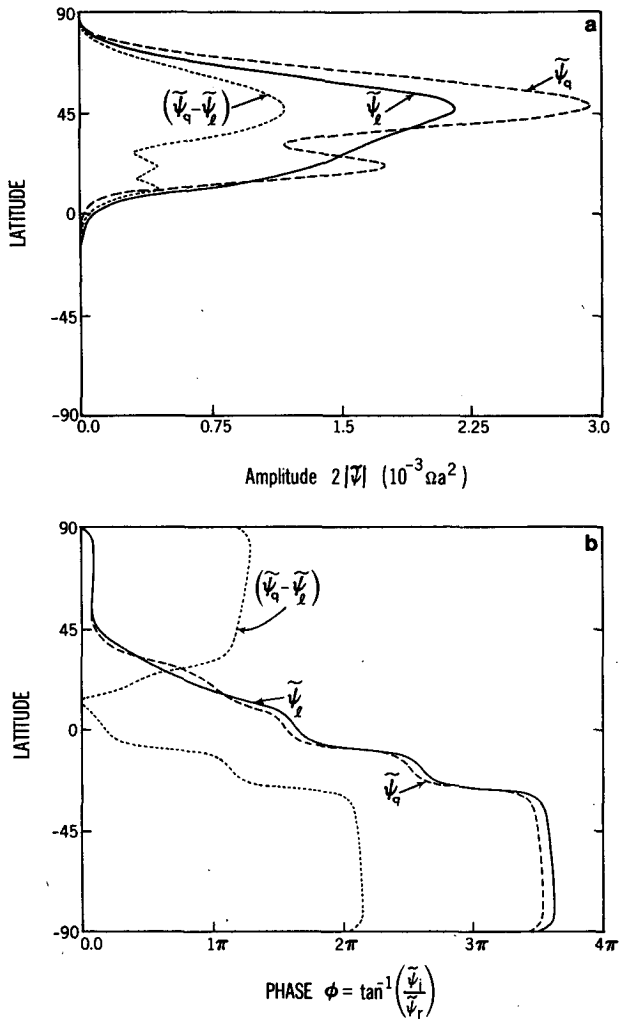


FIG. 3. Meridional structure of the (a) amplitude and (b) phase of $\tilde{\psi}_l$, $\tilde{\psi}_q$ and $(\tilde{\psi}_q - \tilde{\psi}_l)$ shown by the solid, dashed and dotted lines, respectively.

the wave reflected from the tropics and the one emanating directly from the source. If this reflected wave, upon a second reflection from its polar turning latitude, constructively interfered with itself, then one would be exciting a "normal mode" created by partial reflection from the tropics and total reflection from the turning latitude, and one would then expect structure in $|\tilde{\psi}_q - \tilde{\psi}_l|^2$. As it is, the value of $\epsilon$ at which maximum response occurs is determined by the position of the source and not by the requirement that a "mode" trapped between the critical and turning latitude be stationary.

Once a steady state is achieved in the quasi-linear model, the wave response is simply the linear response on the modified zonal flow. How then is one to understand the reflection from the critical latitude in the quasi-linear and not in the linear model? We know that when the WKB approximation is valid, there is

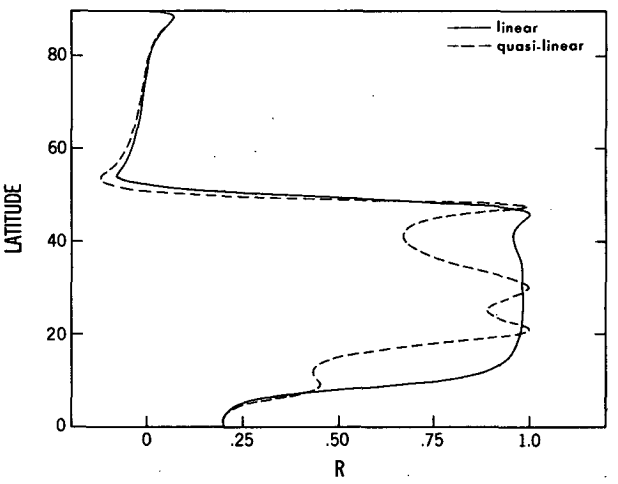


FIG. 4. Meridional structure of the correlation coefficient ($R$). The dashed line distinguishes the quasi-linear case from the linear in regions where the two differ.

no reflected wave and that its breakdown near CL in case of the *linear shear profile* results in essentially complete absorption of the incident wave (Dickinson, 1968; Yamagata, 1976). However, a different wave-behavior near CL is possible in the case of more general continuous flow profiles. We argue that if the WKB approximation breaks down before the wave reaches the region near CL where $\bar{U}$ can be approximated by a linear shear profile, i.e., when there is no overlap of regions where both WKB and (7) are valid, then partial reflection is a possibility. We determine the latitudinal region where the WKB approximation is invalid in our calculation by evaluating $W$ [defined below, cf. (5)] in Mercator coordinates

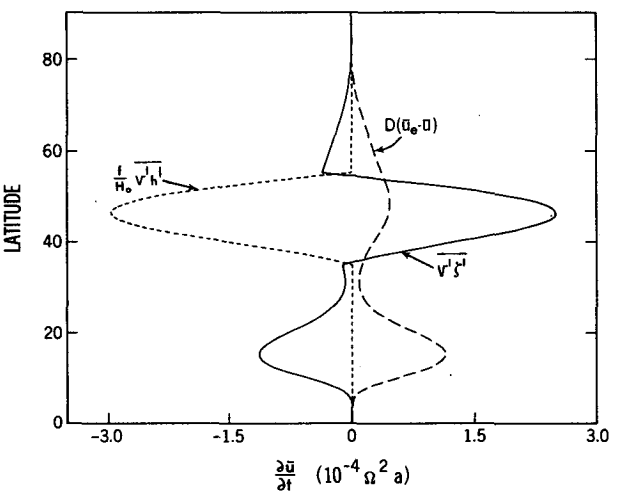


FIG. 5. Meridional structure of the momentum balance in the quasi-linear steady state. The contribution of the eddy momentum flux convergence, relaxation term and form drag is shown along the $x$-axis by the solid, dashed and dotted lines, respectively.

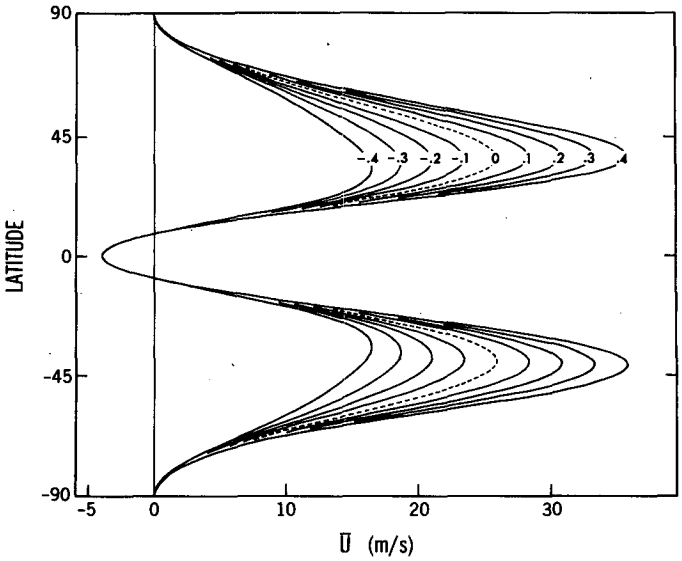


FIG. 6. The nine different zonal wind profiles generated from (11) shown and identified with their $\epsilon$ value. The dashed profile is that of $U1$.

$$W = \left| \left[ l^{-3/2} \frac{d^2}{dy^2} (l^{-1/2}) \right] \right| . \qquad (12)$$

We find that $W > 1.0$, so that the WKB approximation is violated, within 1.2° of the critical latitude in the linear case and within 3.0° in the quasi-linear case. However, the comparison equation (7) is evidently adequate over a much larger latitudinal range in the linear case than in the quasi-linear case. The fractional error $F$, a measure of the invalidity of the linear approximation near the CL, is defined as

$$F = \left| \left( \frac{\alpha}{y - y_c} \right)^{-1} \left[ l^2 - \left( \frac{\alpha}{y - y_c} \right) \right] \right| , \qquad (13)$$

with $\alpha = [\beta_m / \bar{U}_y \cos(\theta)]_{y0}$. We find that $F$ becomes larger than 0.5 at 33.3° north of the CL in the linear case, but at only 4.05° north of the CL in the quasi-linear case. Thus, in the latter case there is little overlap of the regions in which WKB and (7) are both valid, so that Dickinson's analysis which yields complete absorption need not apply.

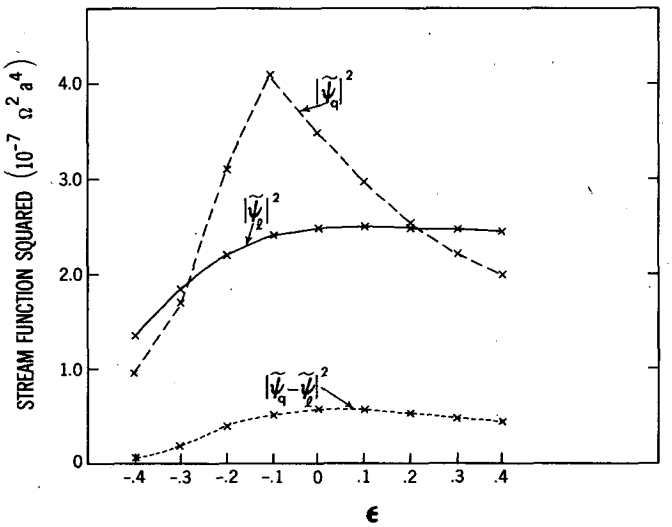


FIG. 7. Domain averages of $|\tilde{\psi}_l|^2$, $|\tilde{\psi}_q|^2$ and $|\tilde{\psi}_q - \tilde{\psi}_l|^2$ shown in the steady state as a function of $\epsilon$ by the solid, dashed and dotted lines, respectively.

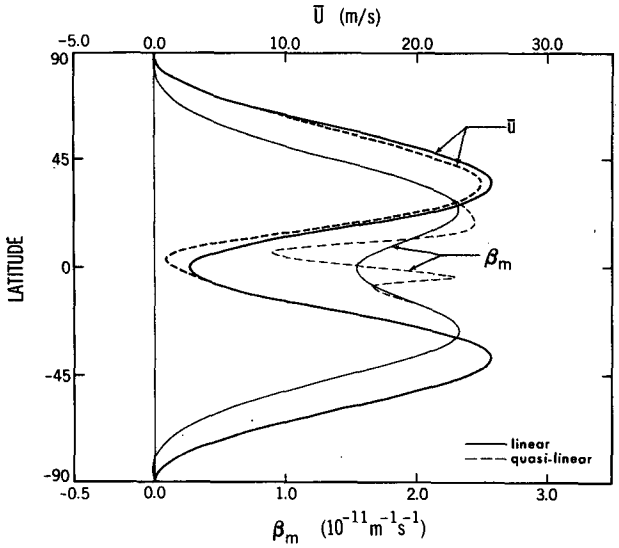


FIG. 8. As in Fig. 1 but for calculations with zonal wind profile $U2$.

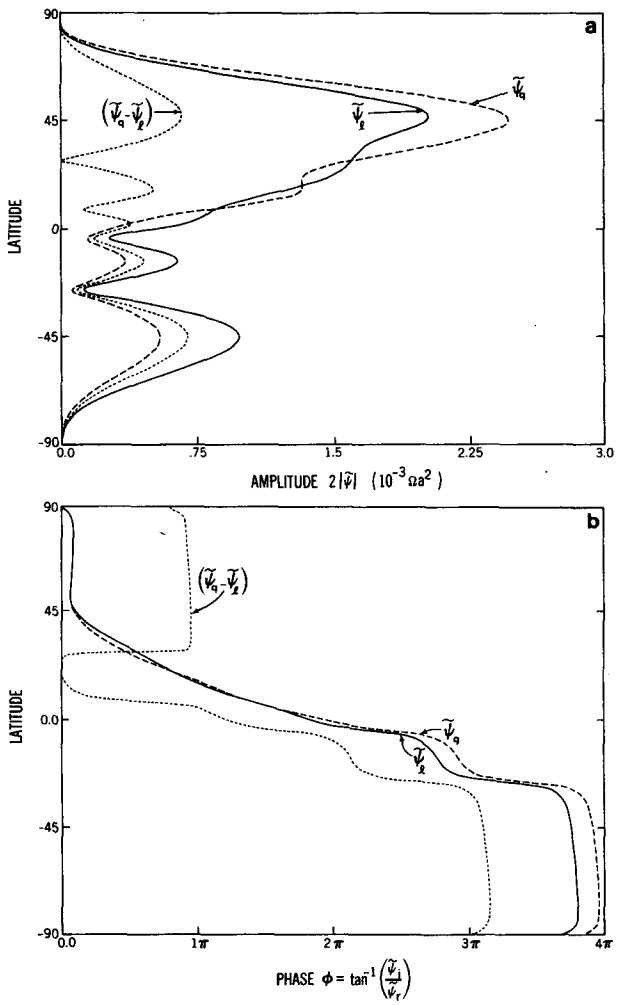


FIG. 9. As in Fig. 3 but for calculations with zonal wind profile $U2$.

### b. *Calculation with U2*

In this subsection, a calculation similar to the preceding one but with zonal wind profile $U2$ (defined earlier) is briefly discussed. Fig. 8 shows $\bar{U}$ and the associated $\beta_m$ in the linear and the quasi-linear steady state. The calculation shows that a much weaker S-shaped structure in $\beta_m$ is obtainable even in the absence of a critical latitude. In the latter case, westerly flow deceleration is noticeable everywhere (even south of the equator) along with modest excursions in $\beta_m$ in equatorial latitudes which result in a slightly modified response in the Northern Hemisphere. In addition, the absence of tropical easterlies enables the Southern Hemisphere to respond to Northern Hemispheric forcing, as shown in Figs. 9a and 9b.

## 5. 15-wave experiment

In this section, we describe calculations in which zonal wavenumbers 1–15 are retained in the forcing and the eddy fields. The Northern Hemisphere topography shown in Fig. 10 and used in these calculations is constructed from the amplitudes of the first 15 waves which were obtained by Fourier analyzing the 1° resolution Scripps topography (Gates and Nelson, 1975). The Himalayan complex has a maximum height of ~5000 m while the Rockies have elevation less than 2000 m. The topography in the Southern Hemisphere is set identical to zero. Following Charney and Eliassen (1949), the topography is multiplied by a constant $\gamma$, $0 < \gamma < 1$, before it is used in Eqs. (2). Results are presented for $\gamma = 0.2$. At this parameter setting, the quasi-linear model approaches a steady state as $t \rightarrow \infty$ for both profiles $U1$ and $U2$. As in the

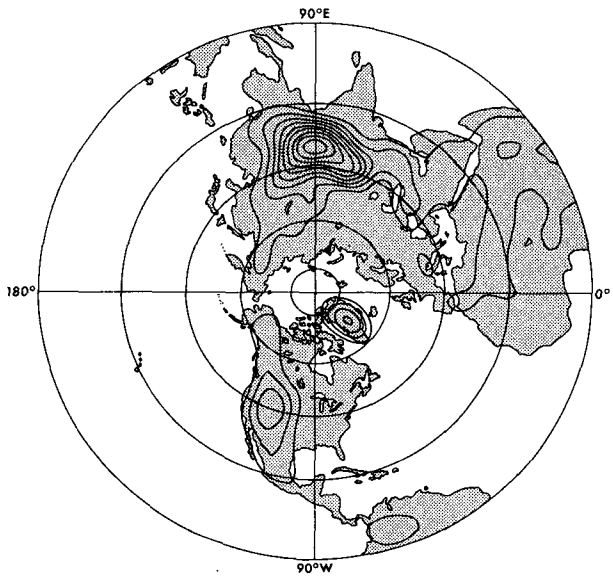


FIG. 10. Northern Hemisphere topography used in the 15-wave calculations. The contour interval is 500 m and the zero contour is not shown. Concentric circles are drawn at intervals of 20° latitude.

previous section, calculations with profiles $U1$ and $U2$ will be described.

### a. Calculation with U1

Fig. 11 shows $\bar{U}$ and the associated $\beta_m$ in the linear and quasi-linear steady state. In the latter case, the S-shaped structure in $\beta_m$ associated with a ledge in the $\bar{U}$ profile near CL is similar to that found in the 1-wave model, and one again expects significant reflection from the tropics. The time evolution of $\beta_m$ in the 15-wave quasi-linear model initialized by the linear model solution shows that the CL attains a reflecting configuration fairly rapidly (within a week); the quasi-linear steady state is realized in ~20 days during which time $\beta_m$ has been through negative values in the vicinity of CL (overreflection).

The Northern Hemisphere eddy streamfunction in the quasi-linear steady state is shown in Fig. 12a. Rossby wave trains emanating from the Himalayan and Rocky Mountains are evident, with the dominant troughs immediately downstream of the mountain complexes showing a southwest–northeast tilt. The Himalayas produce a distinct split wave train, one-half propagating poleward initially and the other equatorward, as in Grose and Hoskins (1979). The northern of the split wave trains changes orientation from northeast to southeast over the Pacific due to reflection off a turning latitude located near 60°N (for $m \approx 3$). The result of subtraction of the eddy streamfunction in the linear case from that in the quasi-linear case is shown in Fig. 12b where the contour interval is a fifth of that in Fig. 12a. Since the two zonal flows are nearly identical except in the vicinity of the critical latitude, this difference field can be thought of as the response to the rather small change in mean winds in the tropics.

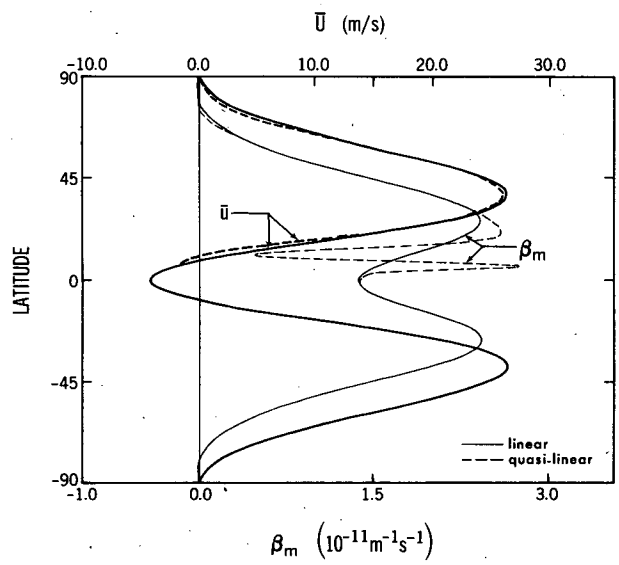


FIG. 11. As in Fig. 1 but for calculations with realistic topography.

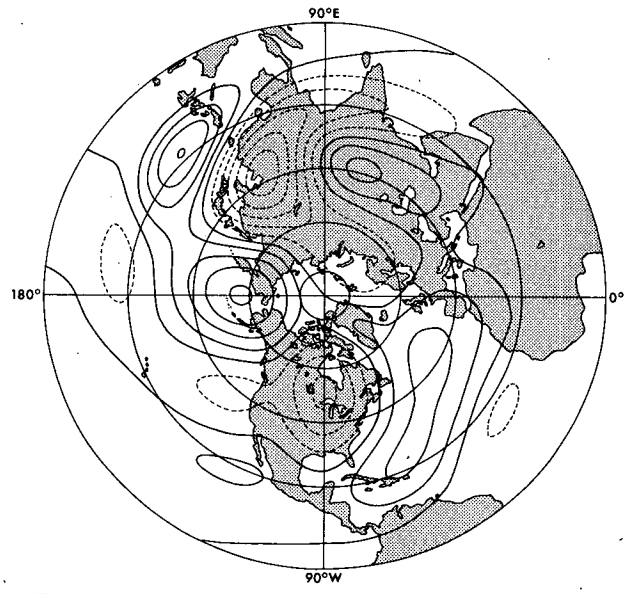


FIG. 12a. Northern Hemisphere eddy streamfunction in the quasi-linear steady state. Dashed (solid) contours represent negative (positive) value. The first solid contour is the zero contour. The contour interval is $1.49 \times 10^6$ m$^2$ s$^{-1}$ ($5.0 \times 10^{-4}$ $\Omega a^2$ m$^2$ s$^{-1}$), which at 45°N is equivalent to 15.63 gpm.

This figure clearly shows the reflections resulting from the encounter of the Himalayan and Rocky wave trains with the critical latitude. The reflected wave train over the Pacific is stronger than the one over the Atlantic because the incident wave is stronger in the former case. The Pacific reflected wave train originates at ~120°E, which is roughly the longitude at which the

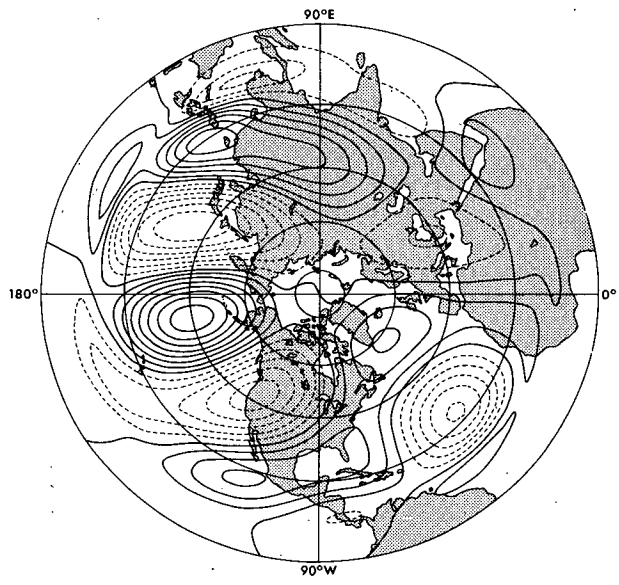


FIG. 12b. Northern Hemisphere difference field resulting from subtraction of the eddy streamfunction in the linear steady state from that in the quasi-linear case. Contours as in Fig. 12a except for the contour interval which is a fifth of that in Fig. 12a.

Himalayan wave train impinges on the critical latitude in this calculation, and attains maximum amplitude near its turning point at 40°N, 165°W. The reflected wave train has sufficient amplitude to modify the linear wave response significantly along its path.

Results from the 1-wave calculation lead one to expect greater sensitivity to mean flow modifications in the quasi-linear than in the linear model. As in the previous section, the sensitivity of the stationary wave response is determined by using the nine different profiles (for $\bar{U}$ in the linear and $\bar{U}_e$ in the quasi-linear models) shown in Fig. 6. In Fig. 13a, the domain average of the *total* form drag is plotted against $\epsilon$ for the linear and the quasi-linear cases; and a similar plot of the individual contribution of the dominant wavenumbers 2–5 is shown in Fig. 13b. The total shows very little difference between the linear and the quasi-linear response, but this is evidently due to considerable cancelation between contributions of different wavenumbers. It is noteworthy that wavenumber 3 does not show the resonant-like behavior seen in the 1-wave quasi-linear model at $\epsilon = -0.1$. This is not because the basic zonal wind in the quasi-linear steady state in the 1-wave experiment is very different from that in the 15-wave experiment, but because of the very different meridional location and structure of the wavenumber 3 component of topography in the latter case. The result is consistent with our understanding of the dependence of the interference between the wave incident on the tropics and the one reflected from the tropical zero wind line on the position of the wave source.

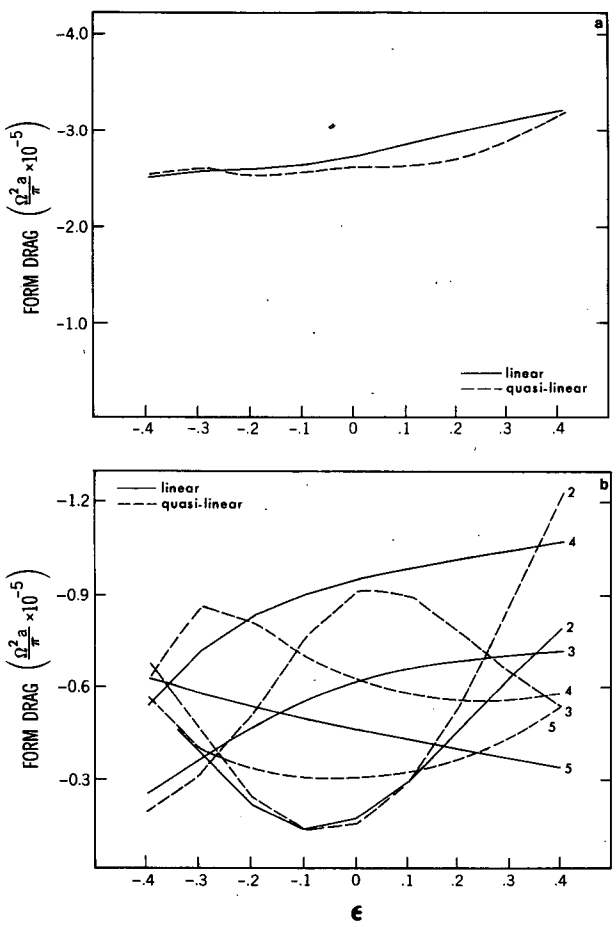


FIG. 13a. Domain averages of *total* form drag shown as a function of $\epsilon$ in the linear (solid) and quasi-linear (dashed) steady states.

FIG. 13b. Individual contribution of the dominant wavenumbers to the domain-averaged total form drag.

### b. Calculations with U2

The calculation described here is similar to the one discussed in Section 5a except that zonal wind profile $U2$ is used instead of $U1$; $U2$ has westerlies everywhere. The resulting difference map, analogous to Fig. 12b, is shown in Fig. 14. The differences between linear and quasi-linear solutions are now considerably smaller and of a different character than before, emphasizing again the importance of the critical latitude. The wave train in Fig. 14 can be traced back to a small difference in the *transmission* of the lower Himalayan wave train as it passes through the slightly modified tropical flow. (The difference in zonal mean winds is much smaller than in Fig. 11, but larger in the tropics than elsewhere because of the small meridional group velocity and resulting large wave dissipation in a region of small $\bar{U}$.) This wave train propagates across the equator into the Southern Hemisphere and returns to the Northern Hemisphere after reflecting off a turning latitude located near 55°S (for $m \approx 3$), not having dissipated entirely during its round trip despite the presence of a linear drag.

### c. Discussion

As stated earlier, all of the results in Sections 5a and 5b were obtained after multiplying the topographic stretching by $\gamma = 0.2$. The resulting wave amplitudes (Fig. 12a) are smaller by a factor of 2 when compared with the orographically-forced component of the stationary eddy field as estimated from general circulation models [e.g., the east Asian trough is ~150 gpm deep in the difference map obtained from "mountain" and "no-mountain" GCMs in Held (1983)]. Furthermore, the comparison of barotropic and baroclinic linear models in Hoskins and Karoly (1981) indicates that $\gamma$ must be of order unity in the barotropic model, in effect blowing upper tropospheric winds over realistic topography, to obtain wave amplitudes comparable with those of the baroclinic models in the upper troposphere. If one is willing to use different dissipation values in (2a) and (2b), one can easily increase the amplitude of the response without changing its structure. For example, if one simultaneously increases the topography by a factor of 2 and $D$ in the zonal mean equation (2a) by a factor of 4, while leaving $D$ in the eddy equation (2b) unchanged, then $\bar{U}$ remains unchanged in the quasi-linear model and the eddy

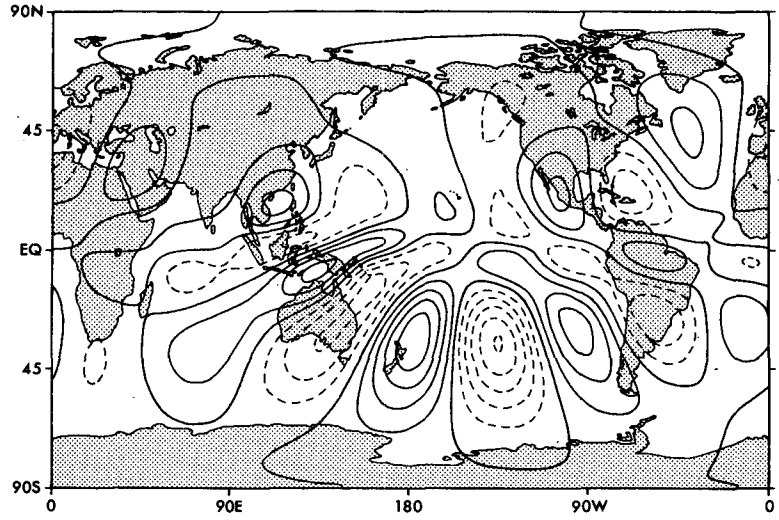


FIG. 14. As in Fig. 12b but for calculations with zonal wind profile $U2$. The Southern Hemisphere difference field is also shown.

streamfunction in the linear and quasi-linear models (and the difference between the two) are simply multiplied by 2. One obtains qualitatively similar results if the fourfold increase in $D$ is confined to the tropics where the most significant mean flow modifications occur.

One of our purposes in examining Eqs. (2) was to see the extent to which the results of Charney and Devore's (1979) beta-plane model carry over to a spherical model in which the mean flow is easterly in the tropics. In Charney and Devore's work, it is the modification of the mean flow in the vicinity of the mountain by the form drag created by the mountain which results in the non-uniqueness of stationary states. An important difference in the present spherical model with uniform damping coefficients is that the bulk of the mean-flow modification occurs in low latitudes and not in the vicinity of the mountains (Fig. 5). As in the 1-wave model, as we increase the strength of the forcing so as to generate more substantial mean-flow modification in midlatitudes, the model's tropical flow becomes unrealistic. While one could try to avoid this difficulty by introducing strong damping of tropical mean flow, one must recognize that this mean flow damping also controls the wave-mean flow interaction responsible for wave reflection. This issue is not pursued further here as the problem is, in fact, more fundamental: the zonal mean flow in low latitudes is maintained against Rossby wave stresses by the Hadley circulation, which acts very differently than a linear relaxation of $\bar{U}$ to a prescribed $\bar{U}_e(\theta)$.

## 6. Meridional structure of $\beta_m$ determined from observations

Monthly mean global circulation statistics compiled by Oort (1983) have been used to compute the meridional structure of $\beta_m$ in the winter (December–February) upper troposphere (300 mb). Monthly mean data are provided at 73 equally-spaced points along each latitude circle and at an equal number of points from pole to pole, covering the period May 1963–April 1973. The zonal velocity field is first averaged over 10 winters and then over longitudes. The resulting profiles of $\bar{U}$ and $\beta_m$ are shown in Fig. 15a. Structure in $\beta_m$, similar to that responsible for wave reflection in our calculations, is seen to be present near the Northern Hemisphere critical latitude. Because of the similarity, it is tempting to argue that this structure is created by the stationary waves forced in the extratropical Northern Hemisphere. The absence of an analogous structure in the Southern Hemisphere is consistent with this interpretation, because of the much smaller stationary wave amplitudes in the Southern Hemisphere. An alternative interpretation that the strong wintertime Hadley cell maintains small absolute vorticities and, therefore, small vorticity gradients cannot be dismissed. Indeed, we suspect that both mechanisms are operating.

Examination of the rawinsonde network during these ten winter seasons reveals the stations reporting upper tropospheric data in the latitude belt (0–10°N) to be very unevenly spaced (Oort, 1978), with not a single reporting station over vast regions of the Atlantic, Indian and the eastern Pacific, but with comparatively more stations reporting over the western Pacific (120–180°E). Therefore, it seems reasonable to average the zonal velocity field over only the "data-rich" longitudes, particularly since this is also the region where the equatorward-propagating Himalayan wave train is incident on the tropics (see Figs. 12a and 12b). Fig. 15b shows $\bar{U}$ and the associated $\beta_m$ when zonal averaging is confined to 120–180°E. The $\beta_m$ profile is broadly similar to that in Fig. 11. One again sees a sharp drop in $\beta_m$ near the latitude where $\bar{U} = 0$ and a positive spike further equatorward.

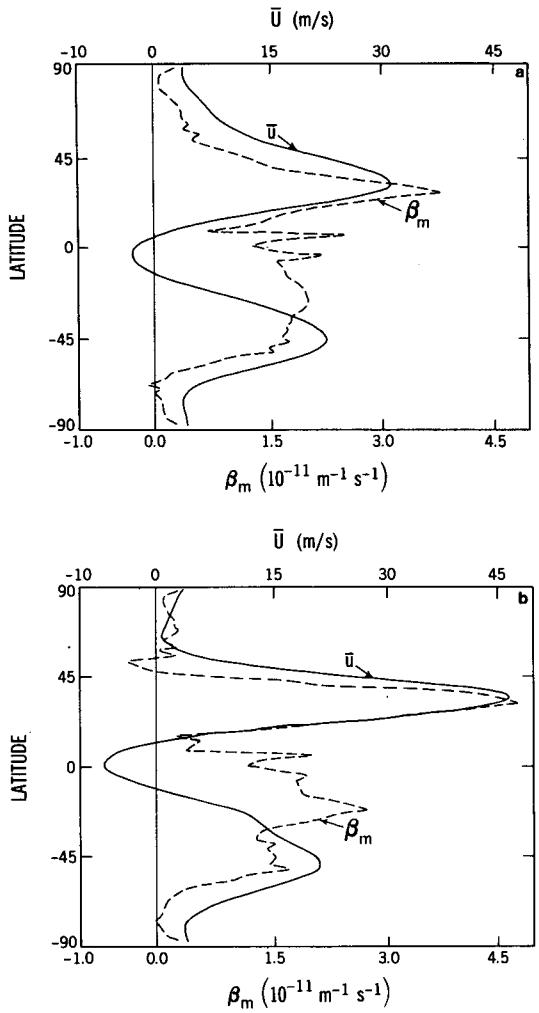


FIG. 15. The 10-year winter averaged $\bar{U}$ profile (solid) and the associated $\beta_m$ (dashed) computed from observations (a) at 300 mb and (b) with longitudinal averaging restricted to the data rich sector (120–180°E).

These features in $\beta_m$, whatever their explanation, can result in significant reflection of incident Rossby waves and are created by small, localized changes in the zonal wind structure. The inadequacies of the observational network force one to be cautious.

## 7. Discussion and conclusions

Results from a barotropic model of topographically forced waves which interact with the mean flow and topography indicate that the strongest of such interactions occur in low latitudes, near the zero-wind line, and that the resulting modifications to the zonal mean wind are quite capable of reflecting a substantial fraction of the incident stationary wave energy, more or less as in the idealized calculation of Geisler and Dickinson (1974). Our results admittedly depend on the damping mechanism in both the eddy and zonal mean equations. In particular, a more realistic treatment of the balance of forces maintaining the mean tropical winds is essential for a satisfactory treatment of the problem. The extent to which these quasi-linear barotropic results are modified by full nonlinearity and three-dimensionality remains to be seen.

Inspection of the observed mean vorticity gradients in the tropics suggests that wave-mean flow interaction similar to that found in the barotropic model may be occurring in the real atmosphere and that Rossby wave reflection is a distinct possibility. If so, it follows that the extratropical stationary wave field is sensitive to the tropical zonal flow, particularly to the presence or absence of easterlies in the upper troposphere at those longitudes at which the dominant wave trains enter the tropics. Variability in quasi-stationary Rossby waves emanating from the tropics may, therefore, have a component due to variability in the reflection properties of the tropical winds as well as a component directly forced by variability in tropical latent heat release.

*Acknowledgments.* We thank Drs. Y. Kurihara, N. C. Lau, S. Manabe, K. Miyakoda and R. T. Pierrehumbert for reading the manuscript and for making several useful suggestions. We would also like to thank Philip G. Tunison and his colleagues for drafting the figures and John N. Conner for photographing them. This work forms a part of the doctoral thesis of S. Nigam who wishes to acknowledge the support of the National Science Foundation through Grant ATM 1727262 A03.

## APPENDIX

### Numerics

Meridional finite differencing of the eddy vorticity equation (2b) on a regular grid results in the difference equation

$$\frac{\partial \tilde{\zeta}_{m,j}}{\partial t} = -\frac{im\bar{U}_j}{a\cos(\theta_j)}\tilde{\zeta}_{m,j} - \frac{im\tilde{\psi}_{m,j}}{a\cos(\theta_j)}\left[\frac{2\Omega\cos(\theta_j)}{a} + \frac{1}{a}\left(\frac{\partial\bar{\zeta}}{\partial\theta}\right)_j\right] - D\tilde{\zeta}_{m,j} - \frac{f_j}{H_0}\frac{im\bar{U}_j}{a\cos(\theta_j)}\tilde{h}_{m,j}, \quad j = 2, N,$$

with the subscript $m$ denoting the zonal wavenumber and $j$ the meridional grid point, and where

$$\left(\frac{\partial\bar{\zeta}}{\partial\theta}\right)_j = -\frac{1}{\Delta^2}\left\{\left[\frac{\bar{U}_{j+1}\cos(\theta_{j+1}) - \bar{U}_j\cos(\theta_j)}{a\cos(\theta_{j+1/2})}\right] - \left[\frac{\bar{U}_j\cos(\theta_j) - \bar{U}_{j-1}\cos(\theta_{j-1})}{a\cos(\theta_{j-1/2})}\right]\right\},$$

and

$$f_j = 2\Omega\sin(\theta_j),$$

$$\theta_j = -\frac{\pi}{2} + (j-1)\Delta,$$

$$\theta_{j+1/2} = \frac{(\theta_{j+1} + \theta_j)}{2},$$

$$\Delta = \frac{\pi}{N}.$$

Here $\tilde{\psi}_{m,j}$ is obtained from $\tilde{\zeta}_{m,j}$ by solving the tridiagonal system

$$\tilde{\zeta}_{m,j} = \frac{1}{(a\Delta)^2 \cos(\theta_j)} \{[\tilde{\psi}_{m,j+1} - \tilde{\psi}_{m,j}] \cos(\theta_{j+1/2}) - [\tilde{\psi}_{m,j} - \tilde{\psi}_{m,j-1}] \cos(\theta_{j-1/2})\} - \frac{m^2}{a^2 \cos^2(\theta_j)} \tilde{\psi}_{m,j},$$

$$j = 2, N,$$

with the boundary conditions $\tilde{\psi}_{m,j} = 0$ at $j = 1$ and $j = N + 1$ and the algorithm of Lindzen and Kuo (1969).

The finite difference version of the zonal mean equation (2a) is

$$\frac{\partial \bar{U}_j}{\partial t} = D(\bar{U}_{e,j} - \bar{U}_j) + \frac{2}{a \cos(\theta_j)} \mathrm{Re}\left\{ \sum_{m=1}^{15} m\left[ i\tilde{\psi}_{m,j}\left( \tilde{\zeta}^*_{m,j} + \frac{f_j}{H_0} \tilde{h}^*_{m,j} \right) \right] \right\},$$

where the asterisk denotes the complex conjugate.

A leapfrog scheme is used for time-stepping, except for the damping terms $-D\zeta'$ in (2b) and $D(\bar{U}_e - \bar{U})$ in (2a), which are carried at the previous time step, e.g.,

$$\frac{(\bar{U}^{t+1} - \bar{U}^{t-1})}{2\Delta t} = (\text{damping term})^{t-1} + (\text{other terms})^t.$$

When inviscid and unforced, *differential* equations (2a) and (2b) together conserve total angular momentum, vorticity, energy and enstrophy. The corresponding *difference* equations likewise conserve the finite difference analog of these quantities, which are:

1) Total angular momentum

$$(2\pi a^2 \Delta) \sum_{j=1}^{J} (\bar{U}_j^{t+1} + \bar{U}_j^t) \cos^2(\theta_j)$$

2) Total vorticity

$$(2\pi a^2 \Delta) \sum_{j=1}^{J-1} \times \left\{ \frac{[\bar{U}_j^{t+1} + \bar{U}_j^t] \cos(\theta_j) - [\bar{U}_{j+1}^{t+1} + \bar{U}_{j+1}^t] \cos(\theta_{j+1})}{a\Delta} \right\}$$

3) Total energy

$$(2\pi a^2 \Delta) \sum_{j=2}^{J-1} \{\bar{U}_j^t \bar{U}_j^{t+1} - 2 \sum_{m=1}^{15} \mathrm{Re}[\tilde{\psi}^{*t}_{m,j} \tilde{\zeta}^{t+1}_{m,j}]\} \cos(\theta_j)$$

4) Total enstrophy

$$(2\pi a^2 \Delta) \sum_{j=2}^{J-1} \left\{ 2 \cos(\theta_j) \sum_{m=1}^{15} \mathrm{Re}[\tilde{\zeta}^{*t}_{m,j} \tilde{\zeta}^{t+1}_{m,j}] + \frac{[\bar{U}_{j+1}^t \cos(\theta_{j+1}) - \bar{U}_j^t \cos(\theta_j)] \times [\bar{U}_{j+1}^{t+1} \cos(\theta_{j+1}) - \bar{U}_j^{t+1} \cos(\theta_j)]}{(a\Delta)^2 \cos(\theta_{j+1/2})} \right\}.$$

Here the superscript $t$ denotes the $t$th time step. Expressions 1)–4) make reference to the fields at adjacent time steps due to the use of the leapfrog time scheme.

## REFERENCES


Beland, M., 1976: Numerical study of the nonlinear Rossby wave critical level development in a barotropic zonal flow. *J. Atmos. Sci.*, **33**, 2066–2078.

——, 1978: The evolution of a nonlinear Rossby wave critical level: Effects of viscosity. *J. Atmos. Sci.*, **35**, 1802–1815.

Benney, D. J., and R. F. Bergeron, 1969: A new class of nonlinear waves in parallel flows. *Stud. Appl. Math.*, **48**, 181–204.

Charney, J. G., and A. Eliassen, 1949: A numerical method for predicting the perturbations of the middle latitude westerlies. *Tellus*, **1**, 38–54.

——, and J. G. Devore, 1979: Multiple flow equilibria in the atmosphere and blocking. *J. Atmos. Sci.*, **36**, 1205–1216.

Dickinson, R. E., 1968: Planetary Rossby waves propagating vertically through weak westerly wind wave guides. *J. Atmos. Sci.*, **25**, 984–1002.

——, 1970: Development of a Rossby wave critical level. *J. Atmos. Sci.*, **27**, 627–633.

Gates, W. L., and A. B. Nelson, 1975: A new (revised) tabulation of the Scripps' topography on a one degree global grid. Part I: Terrain heights. The Rand Corporation, R-1276-1-ARPA, Santa Monica, CA, 122 pp.

Geisler, J. E., and R. E. Dickinson, 1974: Numerical study of an interacting Rossby wave and barotropic zonal flow near a critical level. *J. Atmos. Sci.*, **31**, 946–955.

Grose, W. L., and B. J. Hoskins, 1979: On the influence of orography on large-scale atmospheric flow. *J. Atmos. Sci.*, **36**, 223–234.

Haberman, R., 1972: Critical layers in parallel flows. *Stud. Appl. Math.*, **51**, 139–160.

Held, I. M., 1983: Stationary and quasi-stationary eddies in the extratropical troposphere: Theory. *Large-Scale Dynamical Principles in the Atmosphere*, B. Hoskins and R. Pearce, Eds., Academic Press, 127–168.

Hoskins, B. J., and D. J. Karoly, 1981: The steady linear response of a spherical atmosphere to thermal and orographic forcing. *J. Atmos. Sci.*, **38**, 1179–1196.

Kuo, H. L., 1949: Dynamic instability of two-dimensional nondivergent flow in a barotropic atmosphere. *J. Meteor.*, **6**, 105–122.

Lau, N-C., 1979: The observed structure of tropospheric stationary waves and the local balances of vorticity and heat. *J. Atmos. Sci.*, **36**, 996–1016.

Lindzen, R. S., and H. L. Kuo, 1969: A reliable method for the numerical integration of a large class of ordinary and partial differential equations. *Mon. Wea. Rev.*, **97**, 732–734.

——, and K. K. Tung, 1978: Wave overreflection and shear instability. *J. Atmos. Sci.*, **35**, 1626–1632.

Oort, A. H., 1978: Adequacy of the rawinsonde network for global circulation studies tested through numerical model output. *Mon. Wea. Rev.*, **106**, 174–195.

——, 1983: *Global Atmospheric Circulation Statistics 1958–1973.* NOAA Prof. Paper No. 14, U.S. Govt. Printing Office, Washington, DC.

Tung, K. K., 1979: A theory of stationary long waves. Part II: Quasi-normal modes in a singular waveguide. *Mon. Wea. Rev.*, **107**, 751–774.

Webster, P. J., 1981: Mechanisms determining the atmospheric response to sea surface temperature anomalies. *J. Atmos. Sci.*, **38**, 554–571.

Yamagata, T., 1976: On trajectories of Rossby wave-packets released in a lateral shear flow. *J. Oceanogr. Soc. Japan*, **32**, 162–168.